Pattern Recognition by an Optical Thin-Film Multilayer Model

Xiaodong Li
Gippsland School of Computing and Information Technology
Monash University
Churchill, Victoria, Australia
xiaodong.li@infotech.monash.edu.au

Martin Purvis
Computer and Information Science
University of Otago
Dunedin, New Zealand
mpurvis@commerce.otago.ac.nz

Abstract

This paper describes a computational learning model inspired by the technology of optical thin-film multilayers from the field of optics. With the thicknesses of thin-film layers serving as adjustable "weights" for the computation, the optical thin-film multilayer (OTFM) model is capable of approximating virtually any kind of nonlinear mapping. This paper describes the architecture of the model and how it can be used as a computational learning model. Some sample simulation calculations that are typical of connectionist models, including a pattern recognition of alphabetic characters, iris plant classification, and time series modelling of a gas furnace process, are given to demonstrate the model's learning capability.

Keywords: Artificial Intelligence, Learning algorithms, Pattern Recognition, Thin-films.

1. Introduction

Current works on computational learning, especially those using connectionist approach, have been focused largely on artificial neural networks [1],[2]. Although these models have taken their inspiration from the networks of biological neurons in the human brain, the essence of this form of computation does not require strict adherence to the biological exemplar - architectures that differ significantly from the biological model may exhibit interesting computational properties [2],[3]. With this in mind, we considered optical computing as a potential area worth exploring, since optical systems offer many desirable computational features (e.g., in an optical system, waves can cross without interfering with one another, so optical connections can be made by crossing light waves, and operations on different data can be done in parallel). This paper describes an optical thin-film multilayer model (OTFM) which takes advantage of the optical properties for the purpose of computational learning. The paper is an extended version by Purvis and Li [4], that we place more emphasis on describing the architecture of the thin-film multilayer model, its calculation algorithm, and how it can be used as a computational learning model. Thin film problems are highly nonlinear [5]. A single thin-film layer can be used as a simple processing unit that is highly nonlinear in terms of its input and output mapping. The proposed model consists of multiple thin-film layers each with a different refractive index and thickness. A light beam incident perpendicular to the surface of the multilayer stack is used to propagate information through the structure. The reflectance values (or alternatively, reflection coefficients) of the light incident can be used as the general measurement of the outputs. Inputs can be fed into the model by encoding them into some system parameters such as refractive indices of thin-film layers, and individual layer thicknesses can be used as adjustable parameters.

In Section 2 we first describe the structure of the thin-film multilayer model, its computational algorithm, and how it can be used as a learning model. Section 3 briefly discusses the input encoding scheme. In Section 4 we describe the training procedure adopted for the OTFM learning. Section 5 presents some sample experimental calculations with the simulation model and compares the results to those performed with a conventional neural network architecture. In Section 6 we discuss the experimental results. Finally in the last Section we conclude with a summary and some pointers for future research.

2. The Optical Thin-Film Multilayer Model

We will first consider the optical properties of a single (ideal) thin-film and then go on to consider the case when there are several contiguous thin-films. We assume the material of the thin-film is uniform, mostly transparent, non-dispersive, and can be characterised by a single index of refraction ***ñ***. Its physical configuration can be represented by a plane parallel plate existing in a medium, such as a vacuum, whose index of refraction is equal to **1**.

When a light beam of a single wavelength is incident on such a plane parallel (Fig. 1), the beam is split into two parts - a reflected beam and a transmitted (refracted) beam that enters the material. The respective angles and magnitudes of these newly created beams are determined by the polarization and wavelength of the incident light beam, the angle of incidence of the beam with the plate (thin-film) and the index of refraction of the plate material [6]. Fig. 1 shows the amplitudes of these individual light beam components, with the incident beam shown (on the left) to have an amplitude of ***a***. The amplitude of the reflected beam component (on the left of the Fig. 1) is reduced by the reflection coefficient, ***r***, so its amplitude is ***ar***. Similarly the amplitude of the transmitted component of the beam is reduced by a transmission coefficient, ***t***, and has a resulting amplitude of ***at***. When the transmitted beam inside the plate material reaches the other surface, it is again split up into a reflected beam (which moves back upward towards the original surface) and a refracted beam which

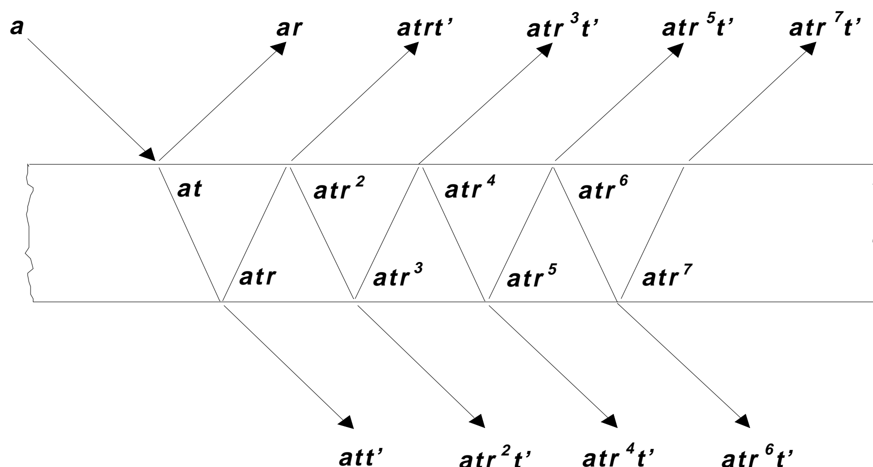

Figure 1. Multiple reflections and refractions at a single thin film layer.

exits the plate. The amplitude of the newly reflected beam is again attenuated by the same reflection coefficient, ***r***, and the amplitude of the newly transmitted beam is attenuated by a second transmission coefficient, ***t'***, associated with light that passes from a refractive material back into the vacuum. As can be seen in Fig. 1, the light beam component inside the plate continues to undergo a (theoretically infinite) number of reflections and refractions, such that there are a number of reflected beams (ar, $atrt'$, atr^3t', atr^5t', atr^7t',..., etc.) and transmitted beams (att', atr^2t', atr^4t', atr^6t', ..., etc.) that come off the top and bottom of the plate.

Since the reflected beams, ar, $atrt'$, atr^3t', atr^5t', etc., are waves, they differ from each other in both amplitude and phase, and the overall reflection of the light beam off the plate will be determined by the multiple-beam interference of this infinite series of reflected component waves [6]. An algebraic expression for this overall reflection of the light beam off the plate can be determined in a straightforward and self-consistent manner if we make the simplifying assumption that the incident beam is perpendicular to the surface of the plate, thereby eliminating the polarization as a factor. The parameters used in this expression are characterised in Fig. 2.

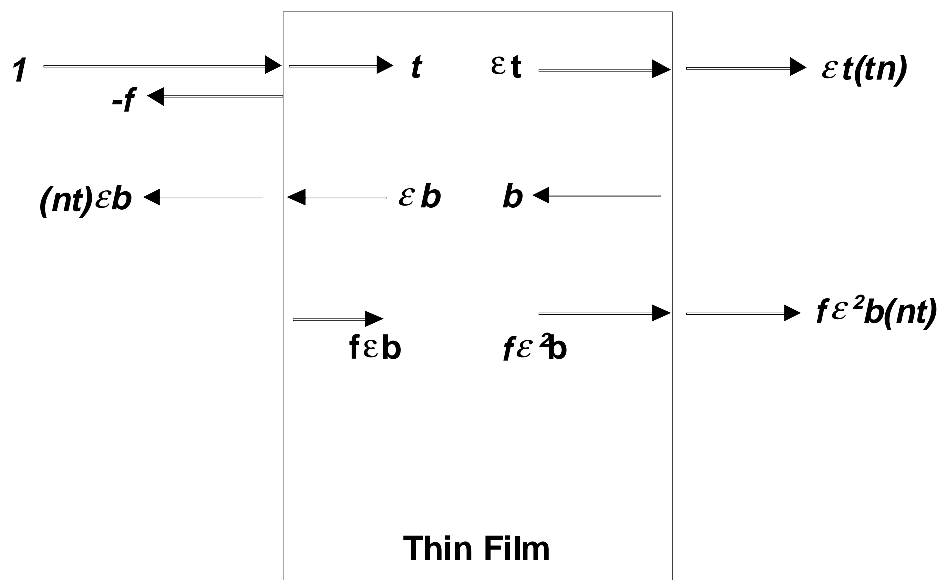

Figure 2. A single thin-film with light incident (**1**) on the left.

A monochromatic light beam (**1** in Fig. 2) with wavelength λ is incident on the left side and, to simplify the discussion, is taken to have an electric field vector amplitude normalized to **1.0** (The light wave also has a magnetic field vector component, but it is sufficient to consider only the electric field vector here. The phase of the wave is customarily incorporated into the description by representing the component as having a complex amplitude). At the left surface of the thin-film, the incident beam is split into a transmitted component and reflected component with amplitudes ***-f*** and ***t***, respectively, where

$$f = \frac{\tilde{n} - 1}{\tilde{n} + 1} \qquad \text{and} \qquad t = \frac{2}{\tilde{n} + 1} \tag{1}$$

$\tilde{n}$ is the complex refractive index of the thin-film, and $\tilde{n} = n + ik$, where n is the ordinary index of refraction and k is the attenuation coefficient. The transmitted beam component with amplitude t now undergoes a phase shift as it travels a distance d (the thickness of the film) up to the right hand surface of the film, so the phase shifted amplitude of the transmitted beam becomes εt, where

$$\varepsilon = e^{i\frac{2\pi\tilde{n}d}{\lambda}} \tag{2}$$

At the right-hand boundary of the film, the beam is again divided up into transmitted and reflected components. The transmitted component that goes off the film at the right-hand surface has an amplitude of $\varepsilon t(tn)$. As the reflected component is one of an infinite series of reflected components at this interface, they can be combined together to represent the interference combination of all of the reflected components by b in Fig. 2; εb is the phase shifted result of this leftward-travelling wave at the inside left-hand surface of the film. At the left-hand surface, the wave with amplitude εb is split into a refracted (transmitted) component with amplitude $nt\varepsilon b$ and a reflected component travelling back to the right with amplitude $f\varepsilon b$. At the right-hand surface, the phase-shifted rightward travelling wave, here with amplitude $f\varepsilon^2 b$, is also split into two components: a reflected component already accounted for by b and a transmitted component with amplitude $f\varepsilon^2 bnt$.

Expressions for the reflection and transmission coefficients of the thin-film can now be taken directly from Fig. 2:

$$r_f = -f + nt\varepsilon b \qquad \text{and} \qquad t_f = (\varepsilon t + f\varepsilon^2 b)nt \tag{3}$$

Eliminating the unknown b from Eq. (3), the complex reflection and transmission coefficients can be given in terms of the refractive index and thickness of the film and the wavelength of the incident light (using Eqs. (1) and (2)):

$$r_f = \frac{-f + \varepsilon^2 f}{1 - f^2\varepsilon^2} \tag{4}$$

and

$$t_f = \frac{\varepsilon(1 - f^2)}{1 - f^2\varepsilon^2} \tag{5}$$

Note that if an input is encoded into $\tilde{\boldsymbol{n}}$ or λ, ε is nonlinear (Eq. (2)). As a result, the output of a thin-film layer, reflection coefficient $\boldsymbol{r_f}$ and the transmission coefficient $\boldsymbol{t_f}$, are highly nonlinear (Eqs. (4) and (5)). Nonlinearity is an important property for the model to carry out more complex computational tasks.

If a second layer is added next to the first one as shown in Fig. 2, $\boldsymbol{r_f}$ will change to some other value, which cannot be calculated from Eq. (4), since the light wave at the incident boundary of the first layer will no longer be **1.0**, and it will change to the total amount of light transmitted through the added layer. Similar change applies to $\boldsymbol{t_f}$ as well. Thus whenever more layers are added, or the thickness of an existing layer is varied, $\boldsymbol{r_f}$ and $\boldsymbol{t_f}$ of each layer will change accordingly.

Now consider the case when several thin-films with different refractive indices have been successively deposited on top of a substrate material to form a multilayer thin-film stack, and a monochromatic light beam, with wavelength λ, incident onto such a multilayer. Fig. 3 shows such a structure with N - 1 layers. **1** represents the total amount of light. Let $\boldsymbol{r_{N-1}}$ denote the (complex) reflection coefficient for the electric field vector in vacuum at the vacuum-multilayer interface, and $\boldsymbol{t_{N-1}}$ denote the transmission coefficient in the output medium at the last boundary surface. The values of these coefficients depend on the refractive indices and thicknesses of all the films in the structure, the refractive index of the output medium, and the wavelength of light.

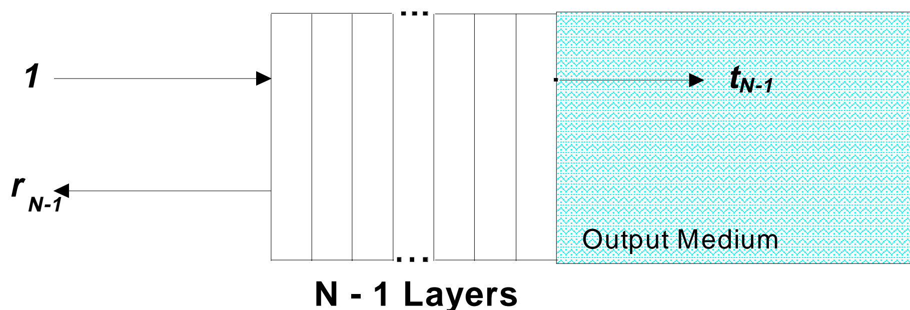

Figure 3. Multilayer thin-film stack of N – 1 layers.

In order to calculate the reflection and transmission coefficients for a multilayer thin-film structure, a recursive approach is used. Imagine an additional thin-film layer, with a complex refractive index of $\tilde{\boldsymbol{n}}_N = \boldsymbol{n}_N + i\boldsymbol{k}_N$ and thickness $\boldsymbol{d}_N$, is brought up to the existing N - 1 layer structure (the imaginary component of the complex refractive index accounts for any absorption of the thin-film material). The distance between the *Nth* layer and the *N*-1 layer structure is going to be zero, but they are shown separated in Fig. 4 for the purpose of explanation.

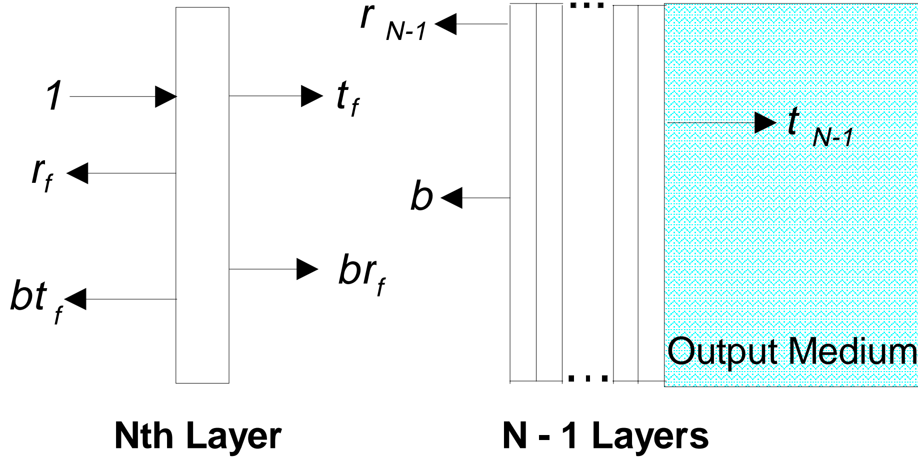

Figure 4. An additional thin-film layer is brought up to a multilayer structure of *N* - 1 layers.

Again, the incident light on the left is taken to have a normalized amplitude value of **1**. Expressions (4) and (5) are used to determine r_f and t_f for the *Nth* layer. Since the light incident on the *N*-1 layer substructure does not have an amplitude of **1.0**, the amplitude of light reflected off its front surface is not its reflection coefficient r_{N-1}, but some other value, which we take to be x. This reflected light with amplitude x is partially reflected by the *Nth* layer back towards the substructure and partially transmitted through the Nth layer out to the left, and these components have amplitudes of xr_f and xt_f, respectively. Since the *N*-1 layer substructure has a reflection coefficient of r_{N-1}, self-consistency requires that the following relations hold:

$$\begin{aligned} r &= r_f + t_f x \\ t &= (t_f + r_f x) t_{N-1} \\ x &= (t_f + r_f x) r_{N-1} \end{aligned} \qquad \textbf{(6)}$$

Eliminating x from the above yields the following expressions for r and t:

$$r = \frac{r_f + (t_f^2 - r_f^2) r_{N-1}}{1 - r_f r_{N-1}} \qquad \textbf{(7)}$$

and

$$t = \frac{t_f t_{N-1}}{1 - r_f r_{N-1}} \qquad \textbf{(8)}$$

r and t are the reflection and transmission coefficients for a *N* layer thin-film stack and r_{N-1} and t_{N-1} are the corresponding coefficients for a *N*-1 layer thin-film stack. Re-labelling these terms so that they correspond to the number of layers in the film stack and substituting in the equations for r_f and t_f

from Eqs. (4) and (5) yields the following recursive expressions for calculating the thin-film stack reflection and transmission coefficients:

$$r_N = \frac{-f_N(1-\varepsilon_N^2)+(\varepsilon_N^2 - f_N^2)r_{N-1}}{(1-f_N^2\varepsilon_N^2)+f_N(1-\varepsilon_N^2)r_{N-1}} \quad \textbf{(9)}$$

$$t_N = \frac{\tilde{n}_N \tau_N^2 \varepsilon_N}{(1-f_N^2\varepsilon_N^2)+f_N(1-\varepsilon_N^2)r_{N-1}} \quad \textbf{(10)}$$

with

$$f_N = \frac{\tilde{n}_N - 1}{\tilde{n}_N + 1} \quad , \qquad \tau_N = \frac{2}{\tilde{n}_N + 1} \quad \text{and} \quad \varepsilon_N = \exp^{i\frac{2\pi\tilde{n}_N d_N}{\lambda}} \quad \textbf{(11)}$$

The recursive expressions shown in Eqs. (9) and (10) provide the means for computing the reflection and transmission coefficients for a thin-film stack of any number of layers. The optical reflectance and transmittance, which are what is ordinarily obtained from optical measurements of thin-film stacks, are directly derived from the reflection and transmission coefficients:

$$R(\lambda) = |r(\lambda)|^2 \qquad \text{and} \qquad T(\lambda) = |t(\lambda)|^2 \quad \textbf{(12)}$$

Note that Eq. (9) $\boldsymbol{r_N}$ is a function, $\boldsymbol{F}$, of a series of system variables,

$$r_N = F(\tilde{n}_0, \tilde{n}_1, \tilde{n}_2, \ldots, \tilde{n}_N, d_1, d_2, \ldots, d_N, \lambda) \quad \textbf{(13)}$$

$\boldsymbol{F}$ is a highly nonlinear function of the refractive indices $\boldsymbol{\tilde{n}_1}$, $\boldsymbol{\tilde{n}_2}$,..., $\boldsymbol{\tilde{n}_N}$, thicknesses of individual layers $\boldsymbol{d_1, d_2, \ldots, d_N}$, λ (i.e. the wavelength used), and $\boldsymbol{\tilde{n}_0}$, the refractive indices of the output medium (the substrate).

Suppose we have a thin-film layer suspended in a vacuum, with refractive index 2.4 and initial thickness close to 0.0. If we increase the layer thickness steadily, in Fig. 5 we can see how the complex reflection coefficient of a single thin-film layer changes in counter-clockwise direction with increasing thickness. The reflection coefficient of the single layer traces out a half-circle within the unit circle (complex reflection coefficients are always within this unit circle with radius 1.0), with respect to its nonlinear association with thickness value, wavelength and refractive index. If somehow we could manipulate such behaviour, e.g., varying the layer thickness to produce the reflection coefficient point towards a specified target point (i.e. a reflection coefficient point somewhere in the unit circle shown in Fig. 5), we might be able to achieve certain kind of learning. The reflection coefficient point of a single thin-film might not be so easily made to reach a specified

target, however when multiple thin-film layers are used, the reflection coefficient of the multiple layer structure would trace out a much more complex dot pattern than the one shown in Fig. 5. Therefore, training the system involves searching through many sets of layer thickness values and eventually finding one that produces the desired reflection coefficients.

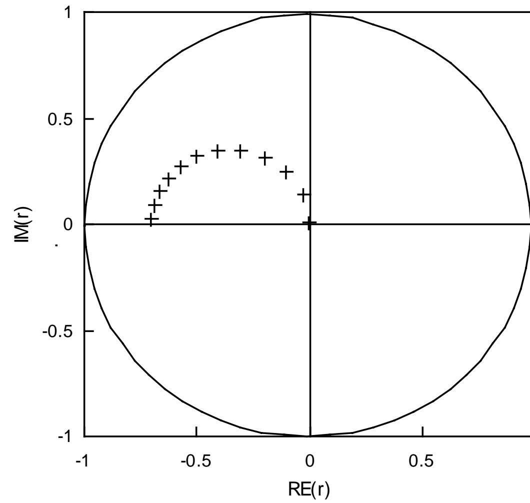

Figure 5. Complex reflection coefficient of a thin-film layer changes when its layer thickness is increased. RE($\boldsymbol{r}$) and IM($\boldsymbol{r}$) denote the real and imaginary components of the complex reflection coefficient $\boldsymbol{r}$.

The optical reflectance value is typically measured by the square of the absolute magnitude of the reflection coefficient given by Eq. (9). Almost any desired spectral characteristic of the reflection can be obtained by choosing a sufficient number of layers with appropriate values of $\boldsymbol{n}$ and $\boldsymbol{d}$ for each thin-film layer.

3. Encoding Scheme

Equations (9), (10) and (11) describe the reflection and transmission coefficients of a N-layered thin-film stack in terms of the N refractive index and thickness values of the layers and the optical wavelength of light. For computational purposes, these coefficients, with real and imaginary values always in the range of -1.0 to +1.0, may be considered to be a generalized output. It is also possible, by means of Eq. (12), to use reflectance and transmittance as generalized outputs and thereby associate computations more directly to conventional optical measurements. Both of these approaches have been used in experiments reported in this paper. With these generalized outputs and for a specified range of optical wavelengths, virtually any desired spectral characteristic of these coefficients can be obtained by choosing a set of thin-film layers with appropriate values of thickness and refractive index.

There are several possible schemes for encoding input information to be used for computational purposes with this model [7]. The approach employed here is to use the indices of refraction of the

various thin-film layers as input values (an alternative approach could use the thicknesses of various layers). Under this scheme if there are to be *M* input values for a computation, then there must be at least *M* thin-film layer available. As shown in Section 4, the thicknesses of the various layers are then used as adjustable "weights" to obtain the desired output.

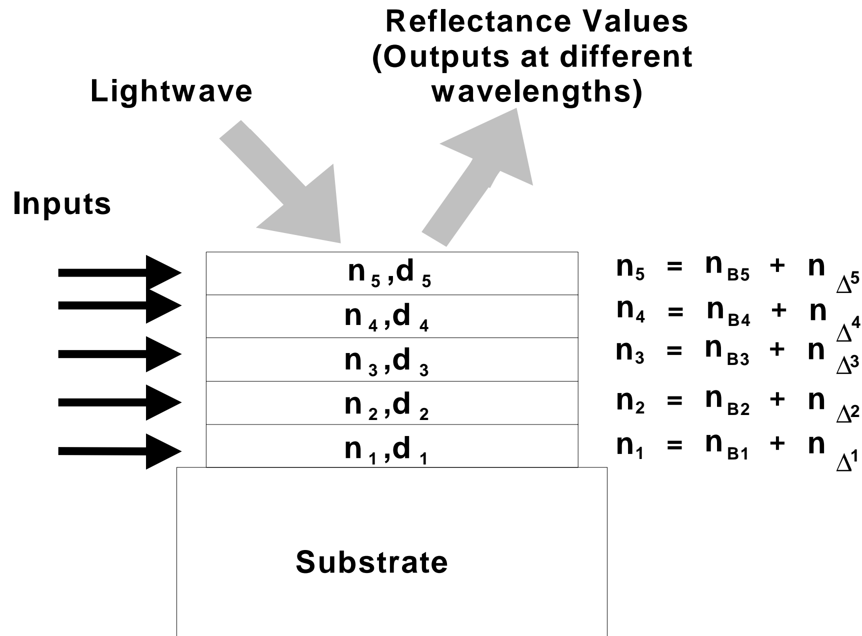

Figure 6. A 5-layer thin-film stack with inputs encoded as incremental values of the refractive indices, $\boldsymbol{n_{\Delta i}}$.

Fig. 6 shows an example of this encoding scheme. A five-layer thin-film stack is shown, each layer characterized by its refractive index, $\boldsymbol{n_i}$, and its thickness, $\boldsymbol{d_i}$. For each layer, $\boldsymbol{i}$, one of the inputs is encoded into an appropriately scaled value of the refractive index, $\boldsymbol{n_{\Delta i}}$, and added to a base value of that layer's refractive index, $\boldsymbol{n_{Bi}}$ (with $\boldsymbol{n_{\Delta}} << \boldsymbol{n_{Bi}}$), to arrive at the layer's index value $\boldsymbol{n_i}$. The value of $\boldsymbol{n_{Bi}}$ are kept large enough relative to the encoded incremental values, $\boldsymbol{n_{\Delta i}}$, to ensure that there is always a substantial variation of the refractive index from layer to layer, irrespective of the value of the input for the layer.

Note that it is not necessary that every layer of the stack be used for input; a thin-film stack could be designed with some extra layers that are not used for encoding input.

The thin-film stack provides output values of the reflection and transmission coefficients for each value of the optical wavelength. One can use a single wavelength for a computation, but it is often more effective to use multiple wavelengths in order to provide better discrimination among the various outputs. When multiple wavelengths are used, an indexing scheme must be set up that maps a desired computational output to a particular spectral responses of the system over the wavelength range.

4. Training Procedure

Training the OTFM involves adjusting the individual layer thicknesses of the stack and then calculating the multilayer reflection and transmission coefficients (or, alternatively, the reflectance and transmittance), using Eqs. (9) - (12). The goal of training in the context of the OTFM is to determine a set of appropriate thicknesses of the thin-film layers in a multilayer model that satisfies the target optical specifications. This procedure can be viewed as the learning process of the OTFM. The training described here is supervised learning [8], where learning is done on the basis of direct comparison of the output of the model, $\boldsymbol{r}(\lambda_k)$ (or $\boldsymbol{R}(\lambda_k)$), with a target output $\boldsymbol{r}_T(\lambda_k)$ (or $\boldsymbol{R}_T(\lambda_k)$). The extent to which the output is acceptable can be measured by the value of a cost function, which generally takes the form:

$$M(x) = \sum_{k=1}^{m} |\,(r_T(\lambda_k) - r(x, \lambda_k)\,|^2 \qquad \textbf{(14)}$$

or

$$M(x) = \sum_{k=1}^{m} |\,(R_T(\lambda_k) - R(x, \lambda_k)\,| \qquad \textbf{(15)}$$

where $\boldsymbol{R} = |\boldsymbol{r}|^2$. $\boldsymbol{x}$ is the vector of design variables including parameters such as individual layer thicknesses; $\boldsymbol{r_T}$ is the target reflection coefficient at λ_k; r is the computed value of the reflection coefficient at λ_k for a particular value of $\boldsymbol{x}$; and $\boldsymbol{m}$ is the number of wavelengths at which outputs are measured.

Training is continued until a configuration of layer thicknesses is found that produces a satisfactory value of the cost function. Note that this thickness configuration is often a result of training using more than one wavelength. The training procedure is an iterative approach that can be described in the following steps:

(1) Initialize the thickness and refractive index of each layer, and assign the initial overall cost $\boldsymbol{M_B} = \infty$. Specify the $\boldsymbol{r_T}$ (or $\boldsymbol{R_T}$) at each λ_k (wavelength). $\boldsymbol{M_B}$ is the current lowest (best) value of the cost function that has been found at each stage of training.

(2) Repeat until the $\boldsymbol{M_B}$ is sufficiently small (or only repeat for a specified number of iterations).

- (2a) Vary thicknesses of some layers (by using an appropriate search algorithm).
- (2b) Calculate $\boldsymbol{r}$ (or $\boldsymbol{R}$) at each λ_k, for all input-target example pairs provided in the training data set.
- (2c) Calculate $\boldsymbol{M}$, the sum of the squares of the error, $(\boldsymbol{r} - \boldsymbol{r_T})$ (or alternatively $(\boldsymbol{R} - \boldsymbol{R_T})$), at each λ_k, for all input-target example pairs, by using the cost function $\boldsymbol{M}(\boldsymbol{x})$ introduced by Eq. (14) or (15).

(2d) If $\boldsymbol{M} < \boldsymbol{M_B}$, then set $\boldsymbol{M_B} = \boldsymbol{M}$, and update the thickness of each layer and other parameters necessary for the later calculations.

(2e) Save and adjust the system parameters for the next round of calculation.

This process continues until a satisfactory solution, a set of appropriate thickness values, is found.

Since training the OTFM involves searching for an optimal set of thickness values and calculating the cost function value for each set of thicknesses, this process is computationally expensive for thin-film structures with many-layers. Instead of exhaustive search through the thin-film thicknesses space, we have adopted two search algorithms for effective training of the OTFM. One is a so called *N-squared Scan* method of Heavens and Liddell [9], and the second one is *Genetic Algorithms* (GAs) of Holland [10]. In our experience, it has been found either search algorithm can sufficiently solve many computational tasks. However when dealing with a complex learning task, using GA first for a good overall search, and then the *N-squared Scan* method for a fine-tuning local search can generally improve the OTFM learning performance to some extent.

The *N-squared Scan* Method works in the following way: if there are *N* layers, initially the first layer thickness is varied and the best thickness result is saved. Then layers 2, 3, 4, etc. are varied in turn in the same fashion. Each time the best combination of thicknesses is retained. After all layers of the stack have been varied, the entire process is repeated, starting this time with layer 2 and ending with layer 1. This variation-of-all-stack-layers process continues, with successive trials beginning with layers 3, 4, etc. Thus if there are *N* layers and we evaluate $\boldsymbol{q}$ different thickness values for each layer, the exhaustive approach would require $\boldsymbol{q}^N$ evaluations, while the *N-squared Scan* approach would require $\boldsymbol{qN}^2$ evaluations. Experience with optical thin-film design has shown that this reduced search-space can still yield acceptable results [9]. In conjunction with the use of the *N-squared Scan* method, we have also developed an algorithmic routine, that takes advantage of previously estimated portions of thin-film stack evaluations for subsequent use, so that new stack evaluations need not re-evaluate the entire stack. This considerably reduces the cost of iterative many-layer film stack evaluations [7].

The second search algorithm adopted, *Genetic Algorithms*, are adaptive searching methods originated by Holland [10] and loosely based on the principles of genetic variation and natural selection - the fittest survive and the worst die off. The appeal of GAs comes from their algorithmic simplicity and elegance as well as from their power to discover good solutions efficiently for difficult high-dimensional problems. In general, a GA performs a multi-directional search, and it encourages information formation and exchange among such directions. It does so by maintaining a population of proposed solutions (chromosomes) for a given problem. Each solution is represented in a fixed alphabet (often binary) with an established meaning. The population undergoes a simulated

evolution: relatively "good" solutions produce offspring, which subsequently replace the "worse" ones. The estimate of the quality of a solution is based on an evaluation function. The existence of such a population gives GAs an advantage over pure hill-climbing methods, as the GA provides for both exploitation for the most promising solutions and exploration of the search space at any time.

Applying Genetic Algorithms to the thin-film model is quite straightforward because of its domain-independency. In general two issues are concerned: the problem encoding and the evaluation function. Eq. (14) or (15) can be used as an evaluation function to calculate the relative fitness of chromosomes in the population during the OTFM training. Problem encoding in a thin-film model is often involved with mapping its system parameters into a genetic representation such as a binary string. Fig. 7 illustrates this encoding process for chromosome segments of 10 bits, which allows the representation of integers {0,1,...,1023}. These integers can be then mapped linearly to a desired interval for thickness values, e.g. $\boldsymbol{d_1}$, $\boldsymbol{d_2}$, **...**, $\boldsymbol{d_N}$ within the range [0.0, 5.0] (each integer is divided by 1023 and multiplied by 5 respectively). Consider the thin-film model where a set of optimal layer thickness values needs to be found to minimize the cost function Eq. (14) or (15). These thickness values are represented by a binary string and the resulting reflection coefficient at each wavelength is evaluated by the cost function Eq. (14) or (15).

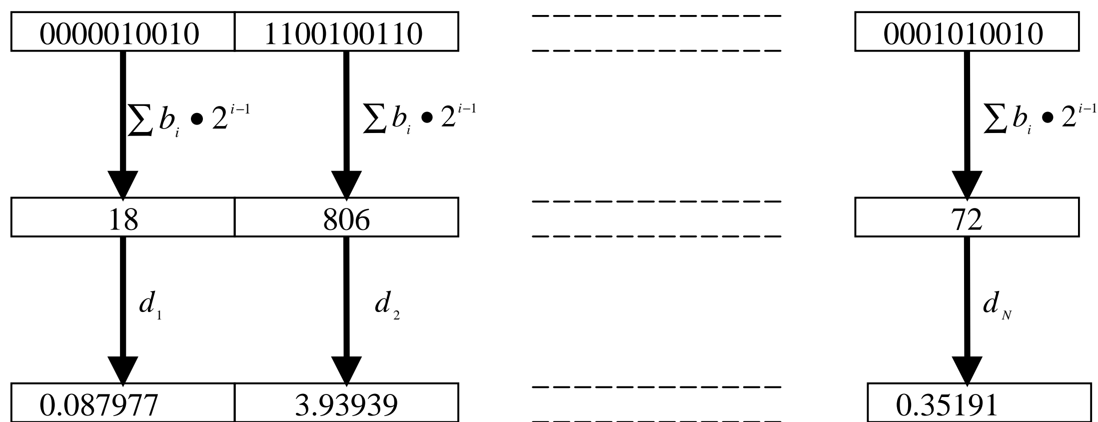

Figure 7. Mapping between chromosome segments and thin-film layer thickness values.

The GA search for an optimal set of layer thicknesses can be defined by the following procedure:

Start: generate initial population of binary bits which represent sets of layer thickness values. For each set of layer thicknesses, the OTFM model evaluates its cost.

Loop through the following steps:

1) Select parents whose genetic make-up contributes to fitter offspring.

2) Produce offspring, using suitable genetic operators (reproduction, crossover and mutation).
3) Evaluate the performance of these offspring.
4) Replace certain parents with new offspring.

5. Experiment

We provide three example simulation calculations with the optical thin-film model to compare the OTFM's learning behaviour with that of other typical connectionist models. The first involves pattern recognition of roman alphabetic characters presented by means of a 5-by-5 grid of pixels. The second example involves discrimination of data for varieties of iris plant into three recognized species [11],[12]. The third example concerns time series prediction associated with the behaviour of a gas furnace [13],[14].

The experiments were conducted on two versions of the OTFM simulation model: a *N-squared Scan* Method Based OTFM run on a 486 PC platform; and a GA-based OTFM simulation model run on a Sun SPARC station 5. In order to train the OTFM, its parameters must be initialized. However, the initial values for these OTFM parameters were simply chosen by trials to find a good starting design, based on our experience and knowledge of optical systems. To examine the performance of the OTFM and compare it with other connectionist models, experiments were also conducted using the same learning examples on a feed-forward neural network model employing the back-propagation learning algorithm [8]. Random samples from the same data sets were used for training and testing. The best training result was selected out of 5 trainings for each data set.

5.1 Pattern recognition of alphabetic characters

A pattern recognition of alphabetic characters was used as an example to demonstrate the OTFM's learning capability. In this experiment, a computational model of an optical thin-film multilayer stack was trained with the 5-by-5 pixel grid patterns representing 'I', 'O', 'C', and 'X' shown in Fig. 8. The thin-film stack was specified to have 25 layers with values of the base refractive index $\boldsymbol{n_{Bi}}$ for each layer alternating between 1.2 for the odd-number layers and 4.0 for the even-number layers. These optical indices were chosen arbitrarily, but lie in the range characteristic of materials used in microwave thin-film optics. The inputs were encoded as small values to be added to $\boldsymbol{n_{Bi}}$ - either 0.0 or 0.4 depending on whether a pixel in the 5-by-5 grid is blank or shaded.

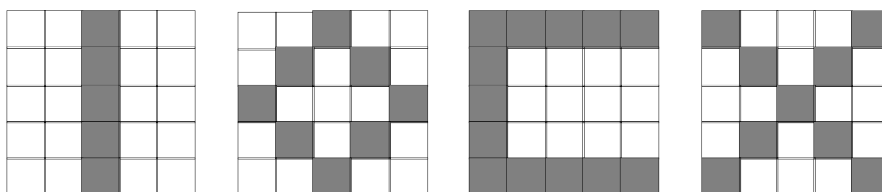

Figure 8. Four 5-by-5 pixel patterns used for training.

Target reflectances for each pattern at 8 different wavelengths ranging from 10.0 μm to 12.8 μm were selected. (For all calculations reported in this paper and in the figures, optical wavelengths and thin-film layer thicknesses are expressed in terms of micrometers. The range of values selected correspond to values for optical thin-film multilayers in the microwave region.) The target reflectance values for the four 5-by-5 grid patterns are shown in Fig. 9.

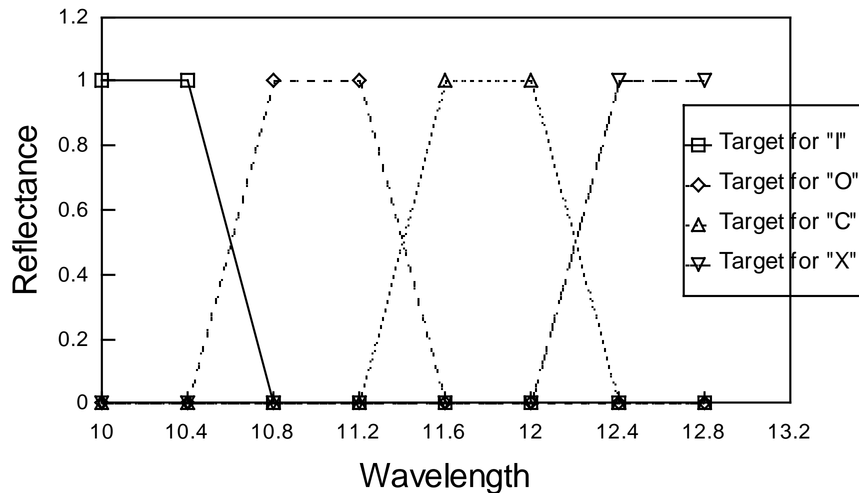

Figure 9. Target reflectances for 'I', 'O', 'C' and 'X'.

The target spectral response for the character 'I' has a peak value of 1.0 in the wavelength range of 10.0 to 10.4, descends to 0.0 at a wavelength of 10.8, and then remains steady at 0.0 out to the wavelength of 12.8. The target response for the character 'O' has peak values in the wavelength range of 10.8 to 11.2 and is zero for wavelengths below 10.4 and above 11.6. The target response for the character 'C' has peak values for wavelengths from 11.6 to 12.0, with zero values below a wavelength of 11.2 and above a wavelength of 12.4. The target response for the character 'X' has peak values for wavelengths between 12.4 and 12.8, with zero values for wavelengths below 12.0.

After the optical thin-film stack was trained using the *N-squared Scan* method, its spectral behaviour when presented with the four training set grid patterns is shown in Fig. 10.

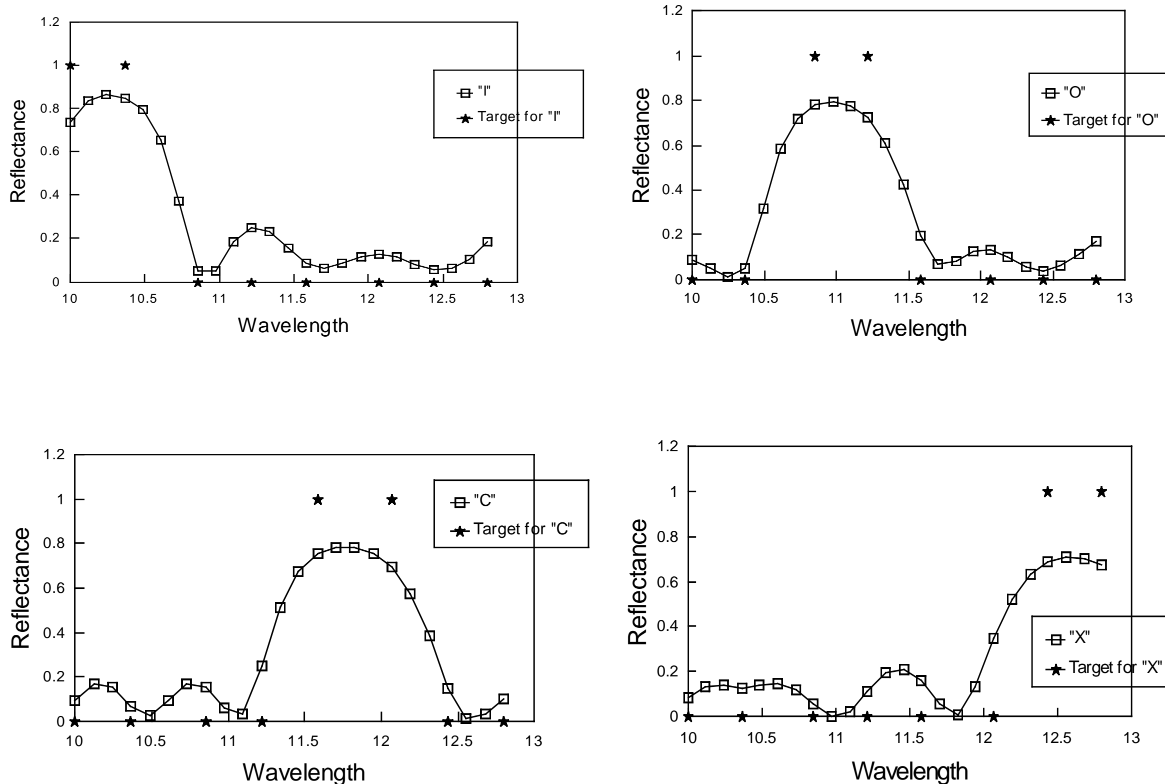

Figure 10. Training result for the four patterns.

As can be seen from Fig. 10, the trained thin-film stack approximates the target curves (although with rounded shoulders).

After training, the thin-film stack was tested for its ability to recognize the bit-patterns in the presence of noise. Four "noisy" versions of the letter 'I' were used for this purpose, and their bit patterns are shown in Fig. 11.

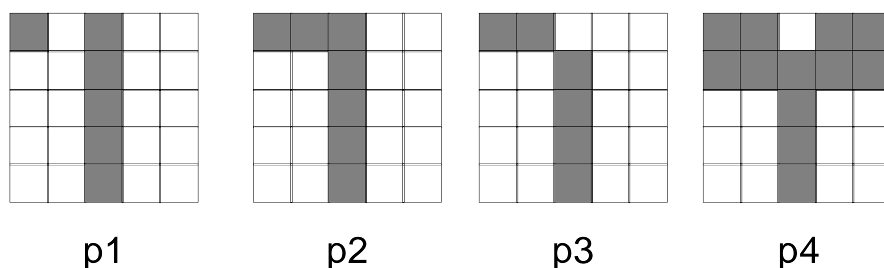

Figure 11. Four "noisy" versions of the letter 'I'.

The first pattern, p1, as shown in Fig. 11, has only one pixel different from the original pattern for 'I' shown in Fig. 8. The patterns p2, p3, and p4 are successively more deviant from the original 'I' grid pattern. The spectral response of the trained thin-film stack to the letter 'I' and the four noisy patterns is shown in Fig. 12.

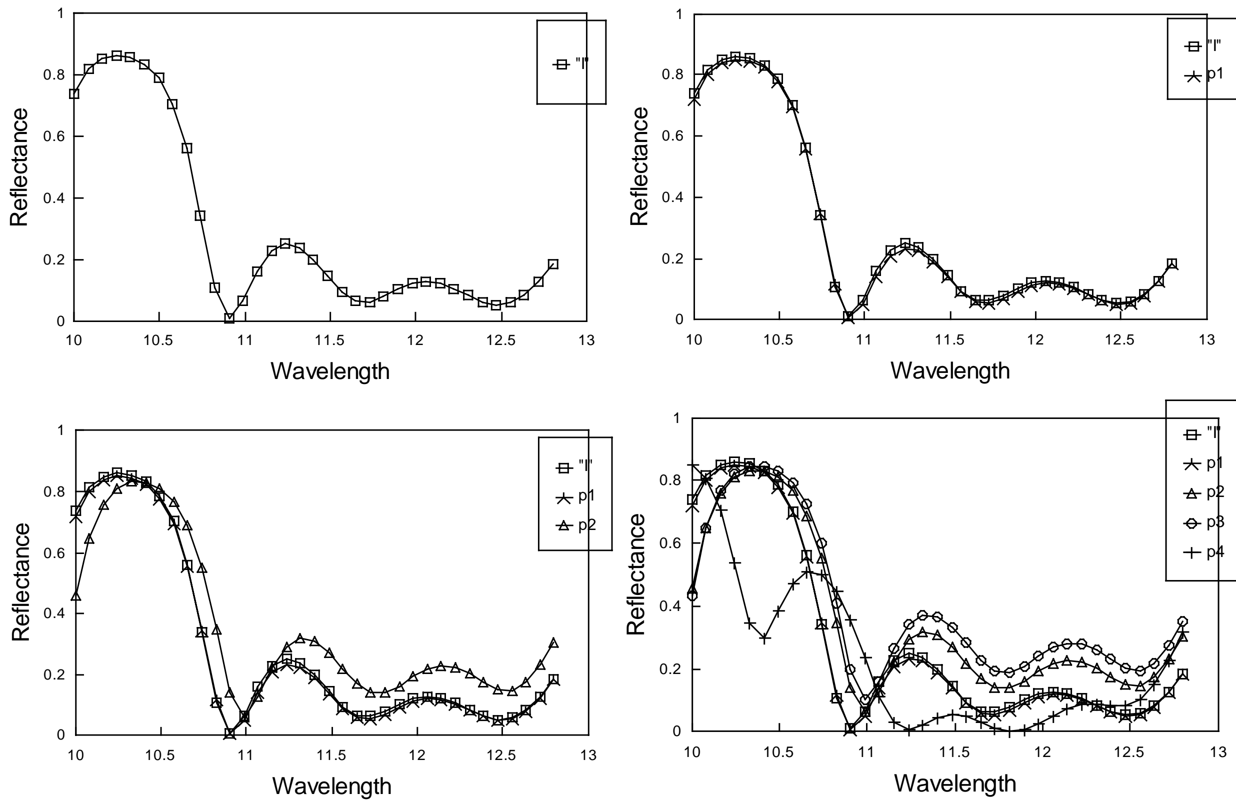

Figure 12. Test result on ‘I’ and its four noisy versions.

The four response curves to the noisy patterns p1, p2, p3, and p4 shown in Fig. 12 show successively greater deviation from the target curve ‘I’ shown in Fig. 9. In particular the response curve for p4 is considerably different from the target for ‘I’. Each of the four noisy patterns have successively larger values of cost function error evaluations (using Eq. (15)). By setting an appropriate tolerance value for cost function evaluations, we can tune the trained thin-film stack to accept some noisy patterns versions of the letter ‘I’ and reject patterns that fall outside the tolerance range.

Thus the optical thin-film model can be trained to recognize certain bit-patterns and can respond correctly even in the presence of noise, just as is the case with conventional neural network architectures.

5.2 Iris Data Classification

The iris data set has been frequently used as an example for discriminant analysis of real data [11]. The data set was collected for three species of iris (setosa, versicolor and viginica) and comprised four measurements (petal length, petal width, sepal length, and sepal width) for 50 samples of each species. One of the species is thought to have arisen as a hybrid species and displays a mixture of features of the other two, making discrimination among the species by means of the measured

properties somewhat difficult [12]. One class setosa is linearly separable from the other two, while the versicolor and viginica are not linearly separable from each other.

Table 1. Target reflection coefficients.

λ	**Class 1**		**Class 2**		**Class 3**	
	r_{RE}	r_{IM}	r_{RE}	r_{IM}	r_{RE}	r_{IM}
5.0	0.2	0.2	-0.5	0.1	0.1	-0.5
5.3	0.3	0.3	-0.4	0.3	0.3	-0.4
5.6	0.4	0.4	-0.3	0.4	0.4	-0.3

For each iris data example used, e.g. {5.1, 3.5, 1.4, 0.2}, it is necessary to scale the values appropriately for encoding into the thin-film system. A thin-film stack of only four layers was selected with values of the base refractive index for each $\boldsymbol{n_{Bi}}$ alternating between 1.2 and 2.5. For this example the complex-valued reflection coefficient was used for the OTFM output, rather than the real-valued reflectance (see Eq. (14)). The training was carried out for the optical wavelength values 5.0, 5.3, and 5.6 μm, and the target reflection coefficient values used are shown in Table 1.

The thin-film stack was then trained with *Genetic Algorithm* approach, using 120 examples (40 randomly chosen from each of the three classes). Chromosome length 60 was chosen, since only 4 layer thicknesses are needed to map into a binary string. After 6 generations, with initial population size 300, crossover probability 0.6 and mutation probability 0.033, the training had the effect of moving the response reflection coefficient points as close as possible to the 3 target points for each optical wavelength value in an effort to separate the collection of output reflection coefficient values as much as possible. Although data from setosa were completely separated from the other two classes, there were a couple of points from versicolor and viginica that always overlapped into each other's regions.

After training, a "winner-take-all" approach [15] was used to set points in the output range to be used for discrimination of samples (during test runs) into the three species. This was accomplished by finding the average values of all the output points at each optical wavelength and for each training class. Thus each of the three species was set to have a set of characteristic values for output reflection coefficients on the basis of the training.

When the test example is presented to the system, it is a matter of calculating the output reflection coefficient for the test example (at each wavelength) and then using the cost function evaluation of Eq. (14) to determine to which species class the example output is closest. Output for thirty novel examples is shown in Figs. 13, 14 and 15. Of the thirty examples only 2 were misclassified by the thin-film system. When the system was given all 150 samples, 5 were classified incorrectly. The

result indicates that the trained model has shown satisfactory classification on the training data set and has also generalized well on novel data from the test data set.

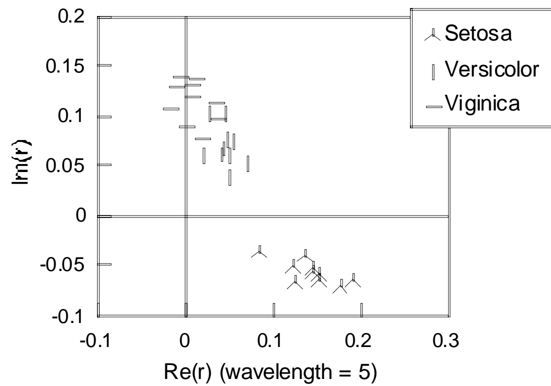

Figure 13. Test results on 30 iris data samples, λ=5.0μm.

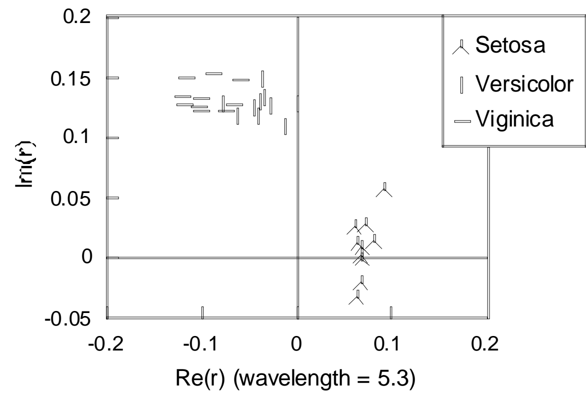

Figure 14. Test results on 30 iris data samples, λ=5.3μm.

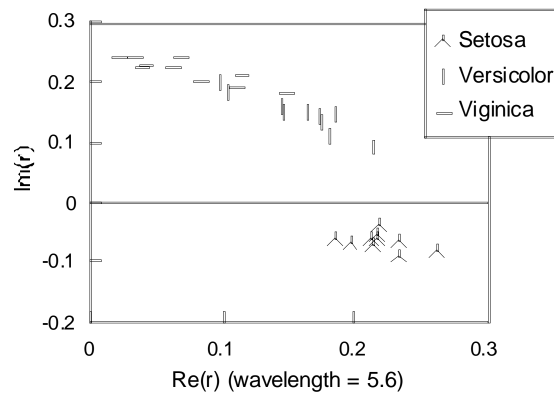

Figure 15. Test results on 30 iris data samples, λ=5.6μm.

Ripley [12], Weiss and Kapouleas [16] reviewed some of the classification results on the iris data using different computational methods. The best neural network (with 3 hidden nodes) training result they had makes 5 misclassifications out of 150 examples. In this research we also used a feed-forward neural network for training on the same training data set, and the trained feed-forward neural network model had the same classification result as that of the trained OTFM: 5 out of 150 incorrect. It is interesting to note that the same 5 examples which were classified incorrectly by the feed-forward neural network model were also classified incorrectly by the OTFM. This is doubtlessly associated with the fact that in both training cases, the same training examples were used: both models reached the same conclusion about the internal relationships among the training data, then classified and generalized in the same way on the test data as well.

5.3. Gas Furnace Time Series

In this experiment, we consider the qualitative modelling of a dynamical process of a gas furnace with a single input (gas flow rate) ***u(t)*** and a single output (CO_2 concentration) ***y(t)*** [13]. In order to train the OTFM to produce an output as close as to the ***y(t)*** (time series prediction), we consider the variables ***y(t-1)***, ***y(t-2)***, ***u(t-1)*** and ***u(t-2)*** as input attributes. Out of 292 data pairs, 250 were used for training and the remaining 42 were used for testing. A 4-layer stack was used for training, with values of the base refractive index for each $\boldsymbol{n_{Bi}}$ alternating between 1.2 and 3.2. The training was carried out on a simulated single optical wavelength 12µm, and the target reflectance values are ***y(t)***s as given in the 250 training data pairs (scaled to be within the range 0.0 to 1.0).

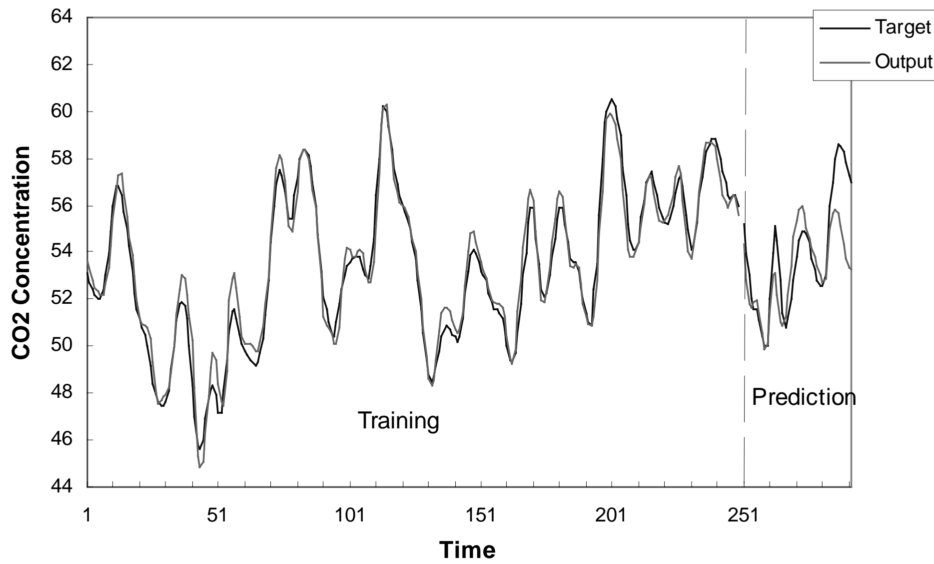

Figure 16. Training result on the Gas Furnace time series data.

The *Genetic Algorithm* approach was used for training. With a population size of 400, a chromosome length of 100 which can be interpreted as 4 thickness values, crossover probability 0.6 and mutation rate 0.033, the training result is shown in Fig. 16. These results compare favourably with training and evaluations performed on the same data set with neural networks [14].

6. Discussion of Results

As illustrated in the previous section, the OTFM training is usually carried out by searching for a set of appropriate layer thickness values to satisfy the target condition. The initial values for parameters $\boldsymbol{n_j}$, $\boldsymbol{d_j}$ and λ (of *j-th* layer) are generally determined by the optical thin-film model designer. The range $0 \leq 4\pi \boldsymbol{n_j d_j}/\lambda \leq 2\pi$ is normally considered [17], since the phase thickness of an individual layer is invariant with respect to a change by the amount $\lambda/2$.

As to accuracy of classification, the OTFM's ability to represent concepts and correctly classify novel examples appears to be comparable with that of the feed-forward neural network model. For

instance, after the OTFM was trained using the 120 examples in the training data set, it was then used to classify the remaining 30 examples in the test data set that are previously unseen to the OTFM, only 2 examples were classified incorrectly. The same result, 2 misclassifications out of the 30 previously unseen data, was obtained from using the feed-forward neural network model employing the back-propagation (but it took somewhat longer to train the neural network model). Note that for both of the training and test data - 150 examples in total, the same 5 examples classified incorrectly by the feed-forward neural network model were also classified incorrectly by the OTFM. Since in both training cases, the same training examples were used, one possible explanation for this similarity in performance is that both trained models reached the same conclusion about the internal relationships among the training data, then classified and generalized in the same way on the test data as well. It has also been demonstrated that the OTFM degrades gracefully when noise in the input pattern increases (see Fig. 12).

Using too many layers and wavelengths may lead to a slow OTFM training. For instance, when using the same initial setup for training the OTFM on the iris data classification employing the GA search method, a 4-layer stack took only 3 minutes to converge to a satisfactory solution, but a 25-layer stack took about 4 hours to converge to a similar solution.

The overall performance of the OTFM on various learning problems used in this research has been shown to be comparable with a feed-forward neural network model in learning many complex computational tasks [7], especially when it is applied to learning problems that are nonlinear and have a moderate number of input attributes (i.e. where it is not necessary to have a large number of layers for encoding the input attributes). In some experiments, the OTFM could achieve a learning that is even better than that of the feed-forward neural network using the back-propagation learning.

7. Conclusion

By using the optical properties of an optical thin-film multilayer model, we have developed a novel computational learning model, **OTFM**, which has shown the learning capability that is typical of a neural network model. We have also used the OTFM in solving of a number of more difficult, as well as real-world learning problems. The performance of the trained OTFM in some of the problem solving is comparable or even better than that of a trained feed-forward neural network model employing back-propagation learning algorithm [7]. Thus for implementing learning tasks it provides an alternative to the neural network models.

The OTFM is still at its initial stages of development and exploration and further experimentation with different learning problems are continuing. The OTFM can stand as a viable computational learning model in its own right, regardless of its feasibility for an optical realization. Nevertheless, such an optical realization would offer the possibility of more or less instantaneous evaluations of the

(trained) thin-film stack. Variations in the refractive index can be achieved for some materials by means of elastooptic, electrooptic, and magnetooptic effects, though the magnitude of the effects is often relatively small [18]. This is an area that may offer promise for additional experimental investigation.

References

[1] G.E. Hinton, Connectionist Learning Procedures, *Artificial Intelligence,* 40 (1989) 185-189.

[2] J.D. Farmer, A Rosetta Stone For Connectionism, *Physica D*, 42 (1990) 153-187.

[3] R. Serra and G. Zanarini, *Complex Systems and Cognitive Processes*, Berlin: Springer-Verlag, 1990.

[4] M.K. Purvis and X. Li, Connectionist Learning Using an Optical Thin-Film Model, in: *Proceedings of the 15th World Congress on Scientific Computation, Modelling and Applied Mathematics - Artificial Intelligence and Computer Science*, vol. 4, eds. by Achim Sydow, Wissenschaft and Technik Verlag, Berlin, 1997, pp. 239-244.

[5] J.A. Dobrowolski and R.A. Kemp, Refinement of Optical Multilayer Systems with Different Optimization Procedures, *Applied Optics*, 29: 19, (1990), 2876-2893.

[6] M. Born and E. Wolf, *Principles of Optic,* New York: Pergamon Press, 1980.

[7] X. Li, *Connectionist Learning Architecture Based on An Optical Thin-Film Multilayer Model*, Ph.D. thesis, University of Otago, Dunedin, New Zealand, 1997.

[8] J. Hertz, A. Krogh, and R.G. Palmer, *Introduction to the Theory of Neural Computation*, Redwood City, CA 94065: Addison-Wesley Publishing Company, 1991.

[9] H.M. Liddell, *Computer-aided Techniques for the Design of Multilayer Filter,* Adam Hilger, Bristol, 1981.

[10] D.E. Goldberg, *Genetic Algorithms in Search, Optimization and Machine Learning,* University of Alabama: Addison-Wesley Publishing Company, Inc, 1989.

[11] E. Anderson, The Irises of the Gaspe Peninsula, *Bulletin of the American Iris Society,* 59 (1935) 2-5.

[12] B.D. Ripley, Statistical Aspects of Neural Networks, in: *Networks and Chaos -- Statistical and Probabilistic Aspects,* Chapman and Hall, London, 1993, pp. 40-123.

[13] G.E.P. Box and G.M. Jenkins, *Time Series Analysis, Forecasting and Control*, Holden Day, San Francisco, 1970.

[14] W. Pedrycz, P.C.F. Lam and A.F. Rocha, Distributed Fuzzy System Modelling, in: *IEEE Transactions on Systems, Man, and Cybernetics*, 25: 5 (1995) 769-780.

[15] A. Hart, Using Neural Networks for Classification Tasks -- Some Experiments on Datasets and Practical Advice, in: *J. Opl. Res. Soc.,* vol. 43, 1992, pp. 215-226.

[16] S.M. Weiss and I. Kapouleas, An Empirical Comparison of Pattern Recognition, Neural Nets, and Machine Learning Classification Methods, in: *Proc. 11th International Joint Conference on Artificial Intelligence*, Detroit, 1989, pp.781-787.

[17] W.E. Case, New Synthesis Method for Optical Thin-Film Coatings, *Applied Optics*, 22: 4 (1983) 4111-4117.

[18] L. Levi, *Applied Optics*, vol II, New York: John Wiley, 1980.